



Operando Observation of Formation and Annihilation of Inhomogeneous Reaction Distribution in a Composite Electrode for Lithium-Ion Batteries

Takashi Nakamura,^{*[a]} Kazuki Chiba,^[b] Mahunnop Fakkao,^[b] Yuta Kimura,^[a] Kiyofumi Nitta,^[c] Yasuko Terada,^[c] Yoshiharu Uchimoto,^[d] and Koji Amezawa^[a]

Inhomogeneous reaction distribution in battery electrodes can be a cause of serious capacity loss and degradation. Therefore, it is important to understand the mechanism of the reaction distribution formation. In this study, formation and annihilation of inhomogeneous charge/discharge reaction in a model LiCoO₂ composite electrode were directly observed by operando two-dimensional X-ray absorption spectroscopy. The reaction distribution was clearly observed, and it was demonstrated that the reacted area became smaller with increasing the current density. The inhomogeneous charged situation remained even after 20 h of the open-circuit rest and the discharge treatments. These results suggested that it is difficult to remove the inhomogeneity once it is formed in a composite electrode.

High-rate charge/discharge cycles may accumulate the inhomogeneity of the state of charge and result in significant capacity losses. The formation of the reaction distribution was strongly affected by the salt concentration in the liquid electrolyte. The expansion and annihilation rates of the charge/discharge reaction did not simply depend on the apparent ionic conductivity of the liquid electrolyte. This suggested that the salt concentration in a composite electrode varies locally by the lithiation/delithiation reactions especially under high-rate operation. Such a local variation of the salt concentration can suppress or facilitate the charge/discharge reactions in a composite electrode.

1. Introduction

Development of high energy density, high power output and reliable batteries is an essential to exploit renewable energies. Especially, high-rate operation of lithium ion batteries is one of the most important technological issues, because of the strong demands for high power output and rapid charging when considering the applications to electric vehicles and large-scale power storages. For these applications, the capacity loss and the insufficient power output often can be serious problems.^[1–3] One of the causes for the poor rate capabilities is the inhomogeneous reaction in the composite electrode.^[4–10] Such a locally non-uniform electrochemical reaction results in the losses of the capacity and the power output. Generally, inhomogeneity of the reaction was caused by the difference of

the rate for each elementary reaction process. Therefore, in order to understand the formation mechanism of the inhomogeneous reaction distribution and to design a high-performance battery electrode capable for a high-rate operation, it is essential to clarify the rate limiting processes of the charge/discharge reaction. For deeply understanding the complicated electrochemical processes in a composite electrode, the visualization of formation and annihilation of the reaction distribution should be very useful.^[7–10] The authors have established two-dimensional X-ray absorption spectroscopy (2D-XAS) and applied this technique to evaluate the distribution of the state of charge (SOC) in the composite electrode.^[7] Although this technique gave us many important information, the measurements in the previous studies were performed only with the electrodes in a disassembled state, *i.e.*, an ex-situ measurements. For further detailed understanding of the formation mechanism of the inhomogeneous reaction distribution in a battery electrode, a direct and real-time observation is desirable.

In this study, operando 2D-XAS was developed and applied to the real-time evaluation of the formation and annihilation of the reaction distribution in a composite electrode. While some real-time observations have been demonstrated as strong and useful tools,^[5,6,11–17] more detailed investigations are still required to understand the electrochemical reactions in real battery electrodes having complicated pathways of ions and electrons. Therefore, in this study, a model composite electrode was proposed and the operando 2D-XAS was applied to investigate the reactions in the model composite electrode. The schematic illustration of the normal and the model composite

[a] Dr. T. Nakamura, Dr. Y. Kimura, Prof. K. Amezawa
Institute of Multidisciplinary Research for Advanced Materials
Tohoku University
2-1-1 Katahira, Aoba-ku, Sendai, 980-8577, Japan
E-mail: takashi.nakamura.e3@tohoku.ac.jp

[b] K. Chiba, M. Fakkao
Graduate School of Engineering
Tohoku University
6-6-1 Aramaki-Aoba, Aoba-ku, Sendai 980-8579, Japan

[c] Dr. K. Nitta, Dr. Y. Terada
Japan Synchrotron Radiation Research Institute
1-1-1, Kouto, Sayo-cho, Sayo-gun, Hyogo 679-5198, Japan

[d] Prof. Y. Uchimoto
Graduate School of Human and Environmental Studies
Kyoto University
Yoshida-nihonmatsu-cho, Sakyo-Ku, Kyoto 606-8501, Japan

 Supporting information for this article is available on the WWW under <https://doi.org/10.1002/batt.201900018>

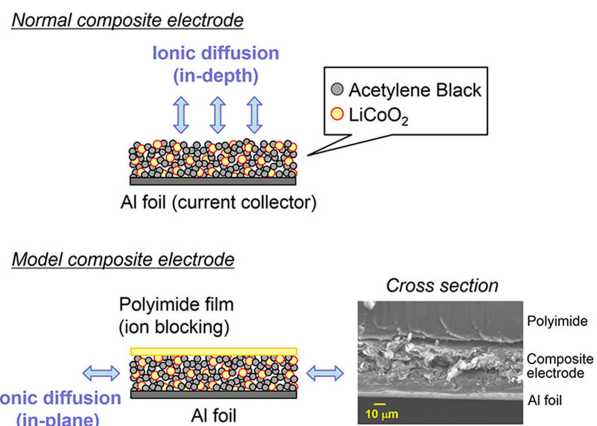


Figure 1. Normal electrode and model composite electrode used in this study.

electrodes are compared in Figure 1. In the model electrode used in this study, as shown in Figure 1, a composite electrode layer was sandwiched by an Al current-collector sheet and a poly-imide insulating sheet. In this model composite electrode, the electronic conduction was sufficiently ensured along both in-depth (about 50 μm) and in-plane directions, while the ionic conduction was limited mostly to along the in-plane direction (about 5,000 μm in maximum). The electrode reaction is considered to proceed from the edge of the model electrode, where the electrode is exposed to a nearly-free liquid electrolyte, to the inside of the model electrode. Then, the inhomogeneous reaction distribution is considered to be formed along the in-plane direction in the model composite electrode, while the uniform reaction distribution can be expected along the in-depth direction, if ionic migration is insufficient in the model composite electrode. The reaction distribution expected in the in-depth direction in the normal composite electrode can be transcribed to the reaction distribution in the in-plane direction in the model electrode. The reaction distribution along the in-plane direction in the model electrode was observed by operando 2D-XAS with the transmission mode at the beam line of BL01B1 and BL37XU in SPring-8, Japan.

2. Results and Discussion

In this work, the reaction distribution in the Li_xCoO₂ composite electrode was investigated by operando 2D-XAS with the transmission mode at the beam-lines BL01B1 and BL37XU in SPring-8, Japan. The measurements were carried out more than 3 hours after the assembly of the cell to ensure the complete soak of the liquid electrolyte and minimize the effect of the solid/electrolyte (cathode/electrolyte) interphase formation during charge. The SOC of Li_xCoO₂ can be determined from the peak top energy of the Co K-edge X-ray absorption spectra, since there exists a one-to-one relation between the peak top energy and the SOC for 0.54 < x < 0.9 in Li_xCoO₂. The reference Li_xCoO₂ specimens were prepared electrochemically from normal LiCoO₂ composite electrodes. XRD patterns, an OCV

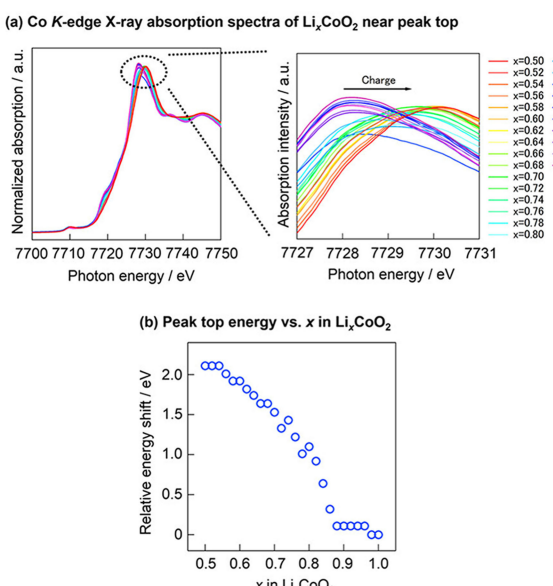


Figure 2. a) Co K-edge X-ray absorption spectra of Li_xCoO₂ and b) the relation between the shift of the peak top energy and x in Li_xCoO₂.

curve, and lattice parameters of reference specimens are summarized in the supporting information. Figure 2 shows Co K-edge X-ray absorption spectra of the reference Li_xCoO₂ specimens and the relative shift of the peak top energy as a function of x in Li_xCoO₂. As Li was de-intercalated from Li_xCoO₂, it was clearly observed that the peak top energy in the spectra shifted to the higher energy. These spectral changes are consistent with earlier works.^[18–20] It was confirmed that the shift of the peak top energy has a one-to-one correlation with the lithium content in Li_xCoO₂ except for the composition ranges around x = 0.5 and 0.9 < x < 1.0. Since the main peak of Co K-edge spectra mainly reflect the structural change around Co, small structural changes are expected in those composition ranges. Although the lithiation/delithiation reaction in Li_xCoO₂ proceeds via two-phase reaction between 0.78 < x < 0.9^[21] or 0.75 < x < 0.94^[22], it is possible to evaluate the SOC of Li_xCoO₂ in the two-phase reaction region if the peak top energy of Co K-edge spectra is used as an indicator.

Schematic procedure of the operando 2D-XAS and data analyses are summarized in Figure 3. For the operando measurements in this study, X-ray absorbance only near the peak top, from 7727 to 7731 eV with a 0.1 eV energy step, was recorded to shorten the measurement time. When the duration time for each photon energy was 0.5 sec, one 2D-XAS measurement was completed within 1 min. Such a quick measurement is useful for the operando SOC observation with a sufficiently high time resolution. The positional resolution was basically determined by the magnification of the optical lens and the pixel size of the CCD detector, which were ×5 and 1.3 μm square, respectively. However, the signal integration for several pixels was needed to obtain a spectrum with a reasonable S/N ratio. The appropriate size of the unit area for the signal was determined by comparing the obtained X-ray absorption spectra from various sizes of the unit area. Figure S3 shows the

2. Results and Discussion

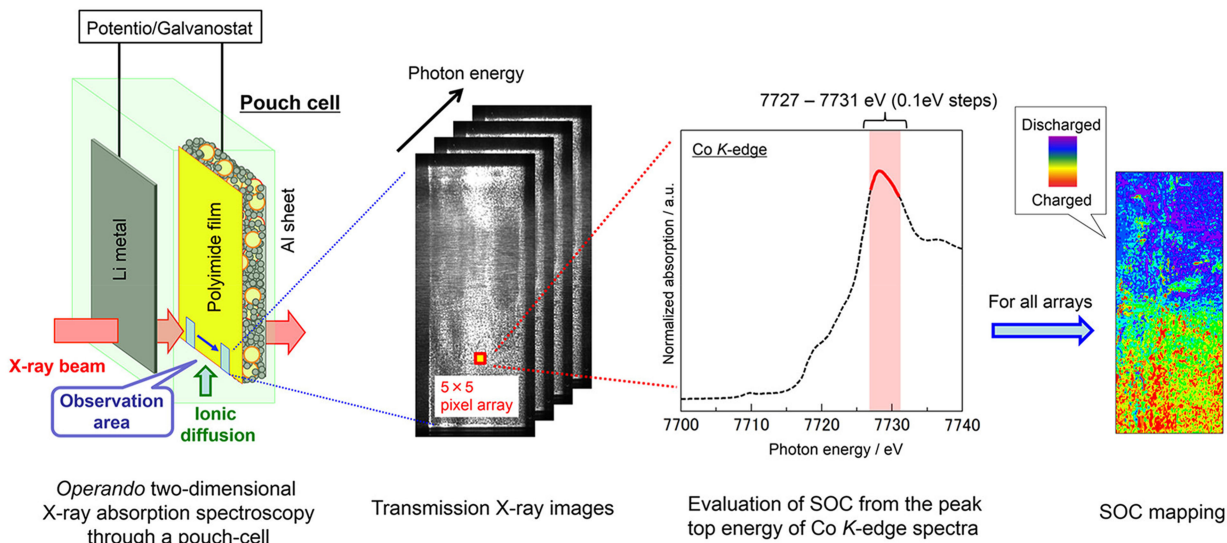


Figure 3. Operando two-dimensional X-ray absorption spectroscopic measurement and the data analysis procedure.

X-ray absorption spectra extracted from 10, 5 and 1 CCD pixel squares, which corresponded to 13, 6.5 and 1.3 μm square, respectively. Clear spectra was obtained even from a unit pixel square. The actual position resolution of the transmission image was about 2–3 μm when a $\times 5$ magnification lens was used. Then, to establish high time and positional resolutions simultaneously, the duration time and the size of the unit for the integration were set to 0.5 sec and a 5 pixel square, meaning about 1 min and 6.5 μm square of the time and the position resolutions, respectively. To minimize the X-ray beam damage, the X-ray irradiation area was changed in each 2D-XAS measurement. Evaluation of the beam damage is summarized in the supporting information.

A movie of the reaction distribution formation in the model composite electrode during the charge with 4.5 mA cm^{-2} (corresponds to 8.0 C) is shown in the supporting information (Movie.avi). Delithiation reaction proceeded from the edge part of the model electrode as expected. As the charge proceeded, the degree of charge at the edge part became deeper and the reacted area expanded to the inner part of the electrode. The progress of the delithiation reaction in the model composite electrode was clearly observed with a sufficiently high time and position resolutions by using the operando 2D-XAS technique developed in this study.

The influence of current density on the reaction distribution formation was investigated. Figures 4-a, -b and c-e show the schematic illustration of the observation area in the model composite electrode, the charge curves, and the SOC mappings of the model electrode, respectively. Here, the current density was defined by the current per the cross-sectional area. The reaction distribution for 4.5, 6, and 8 mA cm^{-2} of the charging current density appear in Figure 4-c, -d, and -e, respectively. These current densities corresponds to 8.0, 10.7 and 14.2 C, respectively. As shown in these figures, the effectively reacted area shrank with increasing the charging current. This tendency

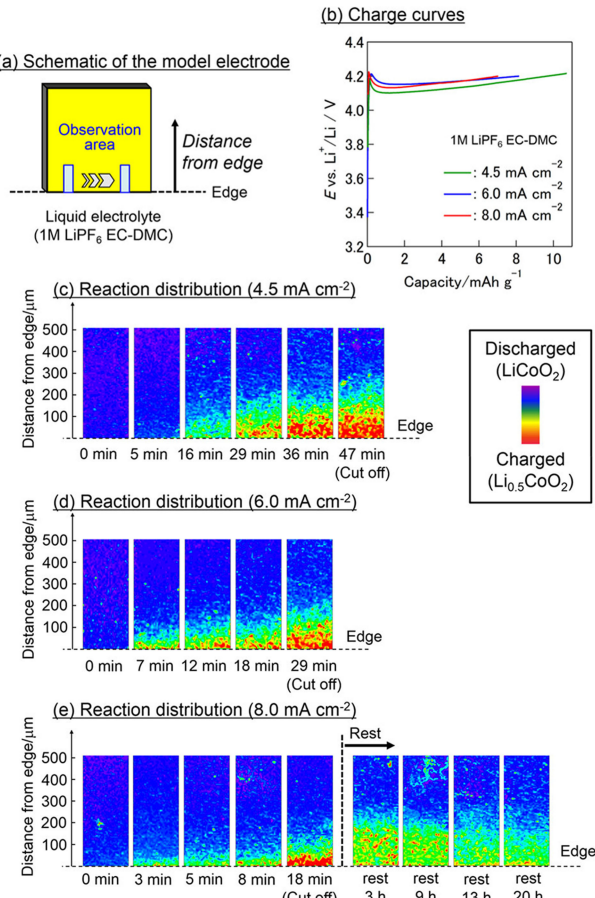


Figure 4. a) Schematic image of the observation area in the model electrode. b) Charge curves observed with the model LiCoO₂ composite electrode for different current conditions. The progress of the reaction distribution in the electrodes for c) 4.5 mA cm^{-2} (8.0 C) charge, d) 6.0 mA cm^{-2} charge (10.7 C) and e) 8.0 mA cm^{-2} charge (14.2 C) and the following relaxation under the open circuit state.

was consistent with that of the charge curve in Figure 4-b, telling that the nominal capacity decreased with increasing the charging current. The cause for the shrinkage of the reacted area with increasing the charging current is probably due to the large overpotential by higher current operation. The rate dependence of the reaction distribution formation demonstrated that the slow ionic diffusion through pores in a composite electrode cause the reaction inhomogeneity under a high-rate operation as suggested in normal composite electrode.^[9,12] The SOC distribution was formed within 200 μm from the electrode edge for the 8 mA cm⁻² charge (Figure 4-e). Since this length is close to the actual thickness of a typical composite electrode in lithium ion batteries, a similar inhomogeneous SOC distribution can be formed in a normal composite electrode for practical lithium ion batteries. For further discussion and theoretical estimation of the reaction distribution formation in a composite electrode, the tortuosity, the shape and size of pores and active materials, and their anisotropy should be took into account.^[23,24]

The relaxation of the reaction distribution under the open-circuit rest treatment is shown in the right half of Figure 4-e. As the open circuit rest proceeded, the charged area gradually extended to the inner part of the electrode, and the degree of charge tended to be averaged. The driving force for this relaxation is considered as the difference of the Li chemical potential which mainly determined by the SOC of Li_xCoO₂. However, the relaxation of the reaction distribution was considerably slow, and the reacted and unreacted areas remained even after 20 hours of the rest treatment. This result suggests that it is difficult to remove the reaction distribution in a composite electrode by the open-circuit rest treatment once it is formed in a composite electrode. One of the possible causes for such a slow relaxation is the small driving force for the chemical diffusion of Li. In the case of Li_xCoO₂, as the OCV curve shows, the SOC dependence of EMF is small even in the solid solution region.^[25] This means the difference of the Li content in Li_xCoO₂ induces only a small difference of the Li chemical potential. Then, a sufficient driving force to fully relax the reaction distribution cannot be expected for Li_xCoO₂, especially, no driving force for the chemical diffusion is expected in the two-phase reaction region of Li_xCoO₂ ($0.75 < x < 0.95$).^[13,21,22]

The annihilation of the inhomogeneous charged area by discharge was also investigated. Figure 5 shows the charge-discharge curves and the formation/annihilation of the reaction distribution. As shown in the charge/discharge curves (Figure 5-a), the electrode potential rapidly dropped at the end stage of the discharge and an irreversible capacity was observed. While the irreversible capacity might be partly caused by the interphase formation on the Li_xCoO₂ surface during the initial charge,^[26–29] this charge/discharge curves suggested that undischarged area might remain in the model composite electrode after the charge/discharge cycle. After the charge, as shown in Figure 5-b, inhomogeneous charged (delithiated) area was formed at the edge part of the model electrode. When discharge reaction started, lithiation reaction proceeded from the edge part to the inner part of the model composite electrode. After reaching the discharge cut-off, the residual delithiated area was clearly observed in the middle part of the

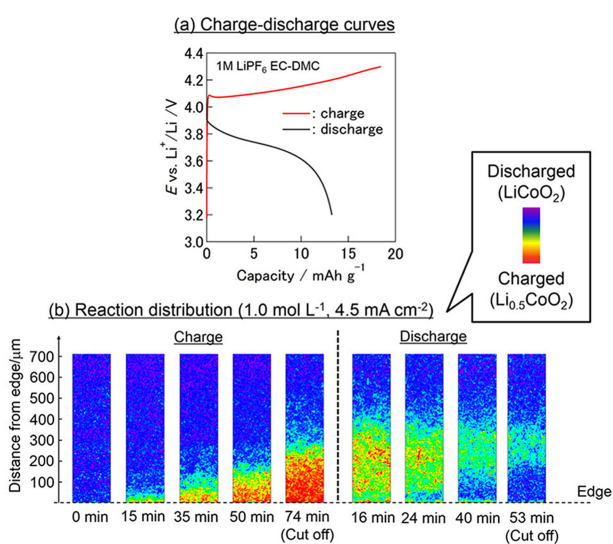


Figure 5. a) Discharge curves observed with the model LiCoO₂ composite electrode. b) Formation/annihilation of the charged area in the model electrode for 4.5 mA cm⁻² of the current density (8.0 C).

model composite electrode. As expected, an irreversible capacity observed in Figure 5-a is partly caused by the formation of unreacted area. These results suggested that it is difficult to fully discharge all of the charged part in a composite electrode if the charge/discharge rate is relatively high to the electrode thickness. Such an inhomogeneity may be formed in each charge/discharge cycle and accumulated in the electrode. In a practical battery electrode, for instance, by the subsequent charge after a cycle, delithiation reaction proceeds from a separator side and expand to the current collector side. During this process, unreacted area formed in the previous cycle is considered to move to the current collector side of the electrode and new unreacted area will be created after the cycle. Then, a high-rate cycling may accumulate the uncharged and/or undischarged area in a composite electrode and lead to a serious capacity fading.

In what follows, the formation mechanism of the inhomogeneous reaction distribution in a composite electrode is discussed based on the equivalent circuit model proposed by Newman, which is shown in Figure 6.^[30] Here, we consider a ladder-type circuit containing the resistance for ionic conduction through the liquid electrolyte (R_{ion}), the resistance for electronic conduction through the conductive aids (R_{ele}), the charge transfer resistance at the electrolyte/active material interface (R_{CT}), and the chemical capacitance of the active material (C_{AM}). According to electrochemical investigations of LiCoO₂, R_{CT} is large at the beginning stage of delithiation ($x \approx 1$), while partly-delithiated Li_xCoO₂ reacts easier than LiCoO₂.^[31,32] It was also suggested that R_{CT} becomes smaller in an electrolyte with a higher salt concentration.^[33] If the R_{CT} decreases due to the changes in the SOC and the salt concentration in our model electrode, LiCoO₂ near the edge part is dominantly delithiated by charging, and the expansion of the reacted area hardly proceeds. As seen in Figures 4 and 5, however, the reacted area fairly expanded from the edge to the inner part of the model

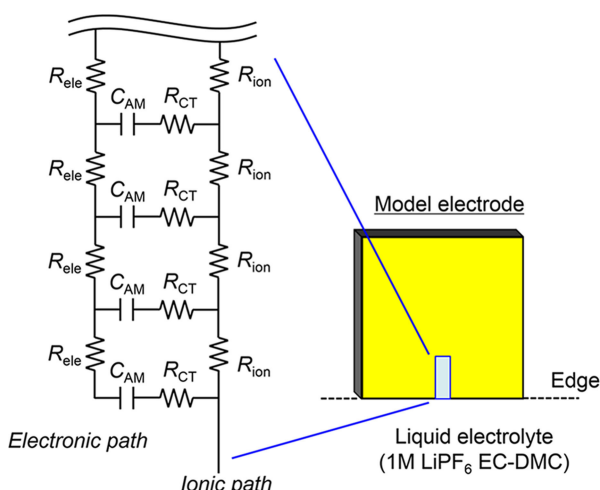


Figure 6. Equivalent circuit for the model composite electrode based on the equivalent circuit model for a porous electrode.^[30]

electrode as the charge proceeded. This indicates that the change of R_{CT} was not significant by the local delithiation reaction. In this case, the expansion of the delithiated/lithiated area is mainly determined by ionic conductivity of the liquid electrolyte, *i.e.* the inverse of R_{ion} . To confirm this hypothesis, operando 2D-XAS was carried out on the battery cells using 0.3, 1 and 2 mol L⁻¹ LiPF₆ in EC:DMC=3:7 as the electrolytes. As reported in ref. 34, we expected that the ionic conductivities of 0.3 and 2 mol L⁻¹ electrolytes were almost the same and half of that of the 1 mol L⁻¹ electrolyte.^[34] Then, the reacted areas in 0.3 and 2 mol L⁻¹ are expected to be comparable and shorter than that in 1 mol L⁻¹, if the salt concentration in the composite electrode is invariant during the charge/discharge. Figures 7-a and b-d show the charge curves and the observed reaction distribution during the charge with 4.5 mA cm⁻². As shown in the figures, the length of the reacted area from the edge was longer in the order of 2 mol L⁻¹ < 1 mol L⁻¹ < 0.3 mol L⁻¹. This order is inconsistent to what we expected from the ionic conductivity of the liquid electrolyte. While experimental or theoretical proofs are not obtained, one plausible explanation for this order is the increase of the local salt concentration in the model composite electrode during the charge. Even if ionic conductivity of the liquid electrolyte is high, two different scenarios can be expected depending on the major ionic carrier, Li⁺ or anion (PF₆⁻ in this case). For instance, during charge, if

Li⁺ diffusion was faster than PF₆⁻ diffusion, Li⁺ ions extracted from Li_xCoO₂ would be smoothly removed to the liquid electrolyte and the local salt concentration stay unchanged. On the other hand, the local salt concentration would increase if PF₆⁻ diffusion is faster than Li⁺ diffusion because the charge neutrality near the Li_xCoO₂ would be kept mainly by the supply of PF₆⁻. In this way, the local salt concentration of the liquid electrolyte in the cathode composite can increase at the place where the delithiation reaction preferentially proceeds, if the charge neutrality is mainly kept by the supply of PF₆⁻ rather than Li⁺ removal. NMR and electrochemical evaluations so far reported agree with our hypothesis *i.e.* the transport number of Li⁺ in the liquid electrolyte is smaller than 0.5 especially in diluted solutions.^[34-37] The local salt concentration change in battery cells during charge/discharge was demonstrated in theoretical calculations and some experiments.^[6,38,39] If the local salt concentration changes like above scenario, the local changes of the salt concentration and the ionic conductivity in our model electrode during the charge can be schematically illustrated in Figure 8. In the figure, the dashed line represents

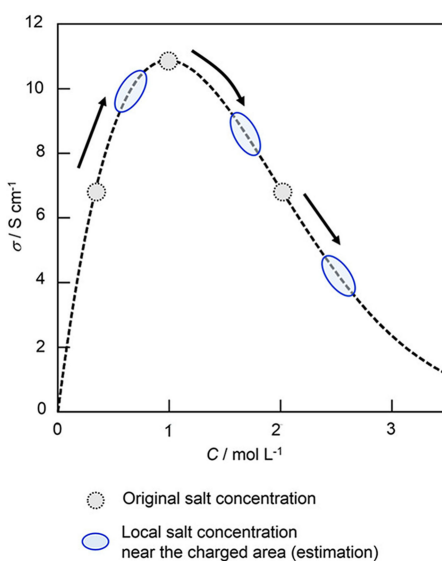


Figure 8. Changes in the local salt concentration and the corresponding ionic conductivity of the liquid electrolyte. The dashed line represents the reported ionic conductivity of LiPF₆ in PC/EC/DMC electrolyte.^[34]

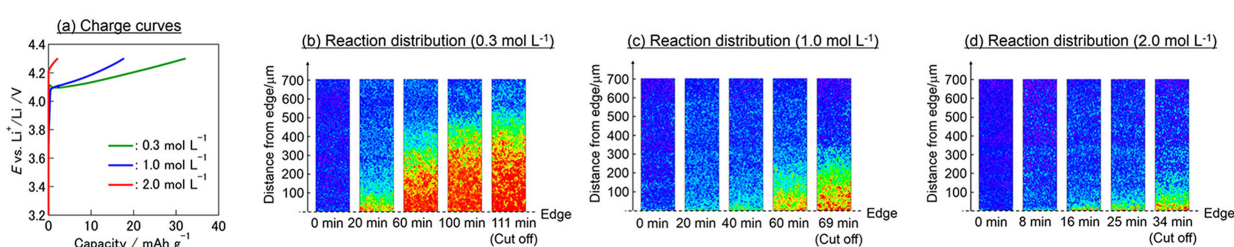


Figure 7. a) Charge curves observed with the model composite electrode in 0.3, 1.0 and 2.0 mol L⁻¹ LiPF₆ EC-DMC electrolytes. The progress of the reaction distribution formation in b) 0.3 mol L⁻¹, c) 1.0 mol L⁻¹ and d) 2.0 mol L⁻¹ LiPF₆ EC-DMC electrolytes.

the ionic conductivity of LiPF₆ in PC/EC/DMC.^[34] If the local salt concentration near delithiated Li_xCoO₂ particles increased during charge, the local ionic conductivity would increase in 0.3 mol L⁻¹ electrolyte and decrease in 1 and 2 mol L⁻¹ electrolytes. Then, the local ionic conductivity can be higher in the order of 2 mol L⁻¹ < 1 mol L⁻¹ < 0.3 mol L⁻¹, and the reactive area is expected to expand from the electrode edge in the same order of ionic conductivity. This suggested that the salt concentration locally varies in the composite electrode accompanied by delithiation/lithiation of Li_xCoO₂ during charge and discharge. Such a variation of the local salt concentration is considered to accelerate or suppress further reaction inhomogeneity during charge/discharge. For the design and the realization of a rate-capable composite electrode, it is necessary to understand microscopic phenomena in the composite electrode including the local variations of the SOC, the salt concentration, and the rates of the charge transfer and the mass transport processes. As shown so far in this study, to deeply understand the charge/discharge reaction mechanism in a practical composite battery electrode, simultaneous evaluations of the reaction distribution and the salt concentration distribution would provide important information.

3. Conclusions

In summary, formation and annihilation of the charge/discharge reactions in a Li_xCoO₂ composite electrode was investigated by operando 2D-XAS. Our operando measurement technique enabled to track the SOC distribution in a composite electrode under the battery operation. It was consequently revealed that the inhomogeneous SOC distribution becomes serious under high-rate operation, and that it is difficult to remove the inhomogeneity by the rest treatments once it was formed in the composite electrode. It was clearly observed that unreacted area was remained in the model composite electrode after charge-discharge. This suggests that high-rate charge/discharge cycling may accumulate the SOC inhomogeneity in the electrode, and cause a significant capacity fading. The present work suggested that the salt concentration can locally vary in the composite electrode by spatially inhomogeneous delithiation/lithiation reactions. The local variation of the salt concentration followed by the local variation of the ionic conductivity in the electrolyte and the electrochemical activity on the active material, can significantly accelerate or suppress the inhomogeneous reaction distribution in real battery electrodes.

Experimental Section

Cell Fabrication

Pouch-type battery cells were used for the operando two-dimensional X-ray absorption spectroscopy in this work. The cells were fabricated as follows. The cathode slurry was made by mixing LiCoO₂:AB:PVDF = 80:10:10 and adding a small amount of 1 methyl-2 pirolydone. The slurry was printed on an Al foil current collector by using a film applicator (Automatic film applicator 542-

AB4, YASUDA SEIKI SEISAKUSHO, LTD.). After drying in an oven, normal LiCoO₂ composite electrodes were obtained. For the model electrode, a polyimide film was placed on the composite electrode layer and then the cathode slurry was dried in an oven at 353 K for more than 80 h. The thickness of the composite cathode layer was about 50 µm. The model electrode was cut into 10 × 10 mm while cooling by liquid N₂. An electrochemical cell was fabricated in a glovebox with an Li metal foil (Honjo Metal Co., Ltd.) as an anode, EC-DMC with 0.3, 1 and 2 mol L⁻¹ of LiPF₆ (EC:DMC = 3:7 in volume, Kishida Chemical Co., Ltd.) as an electrolyte, a polymer separator (Cell-Gard #2500, Polypore International, Inc.), and the model composite electrode. When one edge of the model electrode was immersed to the electrolyte, the electrolyte liquid was smoothly infiltrated into the composite electrode and reached to the other side of the electrode within a few minutes. After the fabrication, the cell was kept for more than 3 h for ensuring the sufficient infiltration of the liquid electrolyte into the electrode. Thereafter, the battery cell was set on the beamline.

SOC reference specimens of Li_xCoO₂ were electrochemically prepared from the normal LiCoO₂ composite electrodes, EC-DMC with 1 mol L⁻¹ of LiPF₆ (EC:DMC = 3:7 in volume, Kishida Chemical Co., Ltd.), and Li metal foil (Honjo Metal Co., Ltd.). After the initial cycle, SOC was controlled by the charge at 0.05 C. Then, Li_xCoO₂ reference samples were taken from the cell after more than 20 h rest treatment, and washed by salt-free EC-DMC (EC:DMC = 3:7 in volume, Kishida Chemical Co., Ltd.).

Operando Two-Dimensional X-Ray Absorption Spectroscopy

Operando two-dimensional X-ray absorption spectroscopy at the Co K-edge was carried out during charge/discharge at the beam line of BL01B1 and BL37XU in SPring-8, Japan. The cell was electrochemically controlled by the Potentio/galvanostat (VersaSTAT 4, Princeton Applied Research). In each charging test, the cut-off voltage was set to 4.2–4.3 V vs. Li⁺/Li. The area of 600 × 1200 µm at the largest near the edge of the electrode was observed with the spatial resolution of approximately 6.5 µm (5 pixels of the CCD camera). The X-ray absorbance was taken in the energy range of 7727–7731 eV with the energy step of 0.1 eV. The exposure time for each energy step was 0.5 sec, and the total measurement time was about 1 min including the waiting time for the motion of the monochromator. The above energy range covers the peak top energy of the Co K-edge absorption spectra of Li_xCoO₂ (0.4 < x < 1). To avoid the beam-damage, the X-ray irradiation area was changed for each measurement.

Acknowledgements

The synchrotron radiation experiments were performed at BL01B1 and BL37XU of SPring-8 with the approval of JASRI (Proposal No. 2014B1301, 2015A2059, 2015B1389, 2015B1991, 2016B1143, 2016A1310, 2016B1194, and 2016B1968).

Conflict of Interest

The authors declare no conflict of interest.

Keywords: in-situ analysis • lithium-ion batteries • operando spectroscopy • reaction distribution • X-ray absorption spectroscopy

- [1] V. Etacheri, R. Marom, R. Elazari, G. Salitra, D. Aurbach, *Energy Environ. Sci.* **2011**, *4*, 3243–3262.
- [2] R. Moshtev, B. Johnson, *J. Power Sources* **2000**, *91*, 86–91.
- [3] J. Ahn, D. Susanto, J. K. Noh, G. Ali, B. W. Cho, K. Y. Chung, J. H. Kim, S. H. Oh, *J. Power Sources* **2017**, *360*, 575–584.
- [4] T. Nishi, H. Nakai, A. Kita, *J. Electrochem. Soc.* **2013**, *160*, A1785–A1788.
- [5] M. Katayama, K. Sumiwaka, R. Miyahara, H. Yamashige, H. Arai, Y. Uchimoto, T. Ohta, Y. Inada, Z. Ogumi, *J. Power Sources* **2014**, *269*, 994–999.
- [6] K. Kitada, H. Murayama, K. Fukuda, H. Arai, Y. Uchimoto, Z. Ogumi, E. Matsubara, *J. Power Sources* **2016**, *301*, 11–17.
- [7] T. Nakamura, T. Watanabe, Y. Kimura, K. Amezawa, K. Nitta, H. Tanida, K. Ohara, Y. Uchimoto, Z. Ogumi, *J. Phys. Chem. C* **2017**, *121*, 2118–2124.
- [8] C. Tian, Y. Xu, D. Nordlund, F. Lin, J. Liu, Z. Sun, Y. Liu, M. Doeff, *Joule* **2018**, *2*, 464–477.
- [9] J. Liu, M. Kunz, K. Chen, N. Tamura, T. J. Richardson, *J. Phys. Chem. Lett.* **2010**, *1*, 2120–2123.
- [10] S. J. Harris, A. Timmons, D. R. Baker, C. Monroe, *Chem. Phys. Lett.* **2010**, *485*, 265–274.
- [11] P. Pietsch, M. Hess, W. Ludwig, J. Eller, V. Wood, *Sci. Rep.* **2016**, *6*, 27994.
- [12] L. Nowack, D. Grolimund, V. Samson, F. Marone, V. Wood, *Sci. Rep.* **2016**, *6*, 21479.
- [13] X. Liu, D. Wang, G. Liu, V. Srinivasan, Z. Liu, Z. Hussain, W. Yang, *Nat. Commun.* **2013**, *4*, 2568.
- [14] M. Ebner, F. Marone, M. Stampanoni, V. Wood, *Science* **2013**, *342*, 716–720.
- [15] J. N. Weker, Y. Li, R. Shanmugam, W. Lai, W. C. Chueh, *ChemElectroChem* **2015**, *2*, 1576–1581.
- [16] Y. Orikasa, T. Maeda, Y. Koyama, H. Murayama, K. Fukuda, H. Tanida, H. Arai, E. Matsubara, Y. Uchimoto, Z. Ogumi, *J. Am. Chem. Soc.* **2013**, *135*, 5497–5500.
- [17] J. B. Leriche, S. Mamelet, J. Shu, M. Morcrette, C. Masquelier, G. Ouvrard, M. Zerrouki, P. Soudan, S. Belin, E. Elkaim, F. Baudelet, *J. Electrochem. Soc.* **2010**, *157*, A606–A610.
- [18] I. Nakai, K. Takahashi, Y. Shiraishi, T. Nakagome, F. Izumi, Y. Ishii, F. Nishikawa, T. Konishi, *J. Power Sources* **1997**, *68*, 536–539.
- [19] W.-S. Yoon, K.-B. Kim, M.-G. Kim, M.-K. Lee, H.-J. Shin, J.-M. Lee, J.-S. Lee, C.-H. Yo, *J. Phys. Chem. B* **2002**, *106*, 2526–2532.
- [20] C. J. Patridge, C. T. Love, K. E. Swider-Lyons, M. E. Twigg, D. E. Ramaker, *J. Solid State Chem.* **2013**, *203*, 134–144.
- [21] G. G. Amatucci, J. M. Tarascon, L. C. Klein, *J. Electrochem. Soc.* **1996**, *143*, 1114–1123.
- [22] M. Menetrier, I. Saadoune, S. Levasseur, C. Delmas, *J. Mater. Chem.* **1999**, *9*, 1135–1140.
- [23] M. Ender, J. Joos, T. Carraro, E. Ivers-Tiffee, *J. Electrochem. Soc.* **2012**, *159*, A972–A980.
- [24] M. Ebner, D. W. Chung, R. E. García, V. Wood, *Adv. Energy Mater.* **2014**, *4*, 1301278.
- [25] H. Tanida, H. Yamashige, Y. Orikasa, Y. Gogyo, H. Arai, Y. Uchimoto, Z. Ogumi, *J. Phys. Chem. C* **2016**, *120*, 4739–4743.
- [26] K. Edström, T. Gustafsson, J. O. Thomas, *Electrochim. Acta* **2004**, *50*, 397–403.
- [27] Y. C. Lu, A. N. Mansour, N. Yabuuchi, Y. Shao-Horn, *Chem. Mater.* **2009**, *21*, 4408–4424.
- [28] M. Gauthier, T. J. Carney, A. Grimaud, L. Giordano, N. Pour, H.-H. Chang, D. P. Fenning, S. F. Lux, O. Paschos, C. Bauer, F. Maglia, S. Lupart, P. Lamp, Y. Shao-Horn, *J. Phys. Chem. Lett.* **2015**, *6*, 4653–4672.
- [29] O. Borodin, X. Ren, J. Vatamanu, A. Von Wald Cresce, J. Knap, K. Xu, *Acc. Chem. Res.* **2017**, *50*, 2886–2894.
- [30] J. Newman, E. K. Thomas-Alyea in *Electrochemical Systems 3rd edition*, John Wiley & Sons Inc. **2004**, pp 517–544.
- [31] M. D. Levi, G. Salitra, B. Markovsky, H. Teller, D. Aurbach, U. Heider, L. Heider, *J. Electrochem. Soc.* **1999**, *146*, 1279–1289.
- [32] K. Dokko, M. Mohamedi, Y. Fujita, T. Itoh, M. Nishizawa, M. Umeda, I. Uchida, *J. Electrochem. Soc.* **2001**, *148*, A422–A426.
- [33] Z. Ogumi, T. Abe, Y. Iriyama, *Solid State Ionics: Trends in the new millennium* **2002**, 3–10.
- [34] L. O. Valoen, J. N. Reimers, *J. Electrochem. Soc.* **2005**, *152*, A882–A891.
- [35] C. Capiglia, Y. Saito, H. Kageyama, P. Mustarelli, T. Iwamoto, T. Tabuchi, H. Tukamoto, *J. Power Sources* **1999**, *81–82*, 859–862.
- [36] J. Zhao, L. Wang, X. He, C. Wan, C. Jiang, *J. Electrochem. Soc.* **2008**, *155*, A292–A296.
- [37] K. Xu, *Chem. Rev.* **2004**, *104*, 4303–4417.
- [38] G. M. Goldin, A. M. Colclasure, A. H. Wiedemann, R. J. Kee, *Electrochim. Acta* **2012**, *64*, 118–129.
- [39] S. A. Krachkovskiy, J. D. Bazak, P. Werhun, B. J. Balcom, I. C. Halalay, G. R. Goward, *J. Am. Chem. Soc.* **2016**, *138*, 7992–7999.

Manuscript received: February 4, 2019

Revised manuscript received: April 2, 2019

Accepted manuscript online: April 2, 2019

Version of record online: April 16, 2019